Structural and Thermodynamic Characterization of the *Escherichia coli* RelBE Toxin−Antitoxin System: Indication for a Functional Role of Differential Stability†

Izhack Cherny,‡ Martin Overgaard,§ Jonas Borch,§ Yaron Bram,‡ Kenn Gerdes,§ and Ehud Gazit*,‡

Department of Molecular Microbiology and Biotechnology, George S. Wise Faculty of Life Sciences, Tel Aviv University, Tel Aviv 69978, Israel, and Department of Biochemistry and Molecular Biology, University of Southern Denmark, DK-5230 Odense M, Denmark

Received May 28, 2007; Revised Manuscript Received August 20, 2007

ABSTRACT: The RelE and RelB proteins constitute the RNA interferase (toxin) and its cognate inhibitor (antitoxin) components of the *Escherichia coli* relBE toxin−antitoxin system. Despite the well-described functionality and physiological activity of this system in *E. coli*, no structural study was performed on the folding and stability of the protein pair in solution. Here we structurally and thermodynamically characterize the RelBE system components from *E. coli* in solution, both separately and in their complexed state. The RelB antitoxin, an α-helical protein according to circular dichroism and infrared spectroscopy, forms oligomers in solution, exhibits high thermostability with a T_M of 58.5 °C, has a considerable heat resistance, and has high unfolding reversibility. In contrast, the RelE toxin includes a large portion of antiparallel β-sheets, displays lower thermostability with a T_M of 52.5 °C, and exhibits exceptional sensitivity to heat. Complex formation, accompanied by a structural transition, leads to a 12 °C increase in the T_M and substantial heat resistance. Moreover, in vivo interaction and protein footprint experiments indicate that the C-terminal part of RelB is responsible for RelB−RelE interaction, being protease sensitive in its free state, while it becomes protected from proteolysis when complexed with RelE. Overall, our findings support the notion that RelB lacks a well-organized hydrophobic core in solution whereas RelE is a well-folded protein. Furthermore, our results support that RelB protein from *E. coli* is similar to ParD and CcdA antitoxins in both fold and thermodynamic properties. The differential folding state of the proteins is discussed in the context of their physiological activities.

Prokaryotic toxin−antitoxin (TA)[1] systems constitute a diverse group of two-protein systems in which one component is a toxin protein and the other is an antitoxin protein that abrogates the effect of the first component (*1*−*3*). When encoded on plasmids, TA systems are considered to function as "addiction modules", ensuring a stable vertical plasmid inheritance by postsegregational killing of cells that become plasmid-free (*1*−*3*). Families of TA systems were also identified on chromosomes of eubacteria and archaea. These systems act by down-regulating the global level of protein synthesis, through the cleavage of mRNA transcripts, leading to cell growth arrest or even cell death (*4*, *5*). However, their physiological role is still under debate. The general opinion suggests that they act as metabolic stress response elements (*2*, *6*−*9*). For instance, physiological studies provided evidence that the *relBE* TA locus acts as a stress response element in bacteria (*10*, *11*). Upon entering nutritional stress conditions, transcription from the *relBE* locus is increased dramatically (*12*). Owing to the proteolytic sensitivity of RelB antitoxin to Lon, RelE toxin is released, consequently eliciting a severe cellular translation arrest (*12*). Conversely, recent study explicitly shows that no selective advantage can be attributed to TA systems under stress conditions, thereby questioning their influence on bacterial fitness and competitiveness (*13*). Recently, TA systems were shown to play a role in the occurrence of bacterial persistence, multidrug tolerance, and biofilm survival (*14*−*16*).

The functionality of both chromosomal and extrachromosome-encoded TA systems is based on the differential metabolic stability of the two system components; whereas the toxins are rather proteolytically stable, the antitoxins display a short half-life, being rapidly degraded by specific proteases (*11*, *12*, *17*−*23*). The instability of the antitoxin allows the subsequent release of the toxins. The difference in the metabolic stability was suggested to stem from their structural and thermodynamic properties. Various studies indicated that the toxins are globular, well-folded, and thermodynamically stable proteins, whereas the antitoxins are less structurally ordered (*22*, *24*−*39*), making them more available to ATP-dependent proteases (*40*).

The *Escherichia coli* RelBE system is one of the most extensively studied TA systems. Homologues of this system were identified in bacterial and archeal chromosomes and plasmids (*10*, *16*, *17*) and shown to be functionally active. In addition, on the basis of the low sequence similarity or

† This work was supported by the Danish Centre for mRNP Biogenesis and Metabolism.

* To whom correspondence should be addressed. Phone: + 972-3-640-9030. Fax: +972-3-640-5448. E-mail: ehudg@post.tau.ac.il.

‡ Tel Aviv University.

§ University of Southern Denmark.

[1] Abbreviations: CD, circular dichroism; FT-IR, Fourier transform infrared; MALDI-TOF, matrix-assisted laser desorption ionization time-of-flight; SEC, size exclusion chromatography; TA, toxin−antitoxin; TM, thermal melting.

10.1021/bi701037e CCC: $37.00
Published on Web 10/09/2007

structural resemblance of their toxins, the *dinJ*−*yafQ*, *yefM*−*yoeB* (*E. coli*), *pas* (plasmid pTF-FC2), *parDE* (plasmid RK2), and *higBA* (plasmid Rts1) systems were considered to belong to the *relBE* TA superfamily as well (*2*, *41*, *42*). The activity of RelE is expressed in the cleavage of mRNA transcripts promoted by RelE binding at the ribosomal A-site. The cleavage occurs at the second position of the A-site codon, preferentially in stop codons (UAG, UAA, UGA), but in sense codons as well (UCG, CAG). This activity leads to global inhibition of protein synthesis in the cell and eventually to cell growth arrest (*10*, *29*, *43*).

A detailed structure of the RelBE complex from the archaeon *Pyrococcus horikoshii* OT3 (aRelBE) was resolved by X-ray crystallography (*29*). Accordingly, the aRelB/aRelE complex forms a 2:2 heterotetramer, where aRelE is a globular protein, well-folded, with a structural content of 33% α, 34% *β*, and 33% loops. Its structure shows some resemblance to those of microbial RNases (*6*). The aRelB antitoxin, which is predominantly an α-helical protein (60% α-helix), is mainly composed of two helical regions separated by a long turn. It clearly lacks a hydrophobic core and wraps around the aRelE toxin in the complexed state, suggesting that it is less structurally ordered in the free or monomeric state. The aRelB−aRelE interaction was assumed to simply act to enlarge the volume of the toxin to disable it from entering into the ribosome A-site (*29*). Protein sequences wrapping around their partner is a rather common occurrence among natively unfolded regions. This binding is usually accompanied by a conformationally induced fit (also known as "coupled folding and binding"), leading to stabilization of the fluctuating disordered region. The thermodynamic driving force is attributed to a favorable enthalpic contribution, which compensates for the lack of a hydrophobic core (*44*−*46*).

In this study we examined the structural, thermodynamic, and oligomerization properties of the RelB antitoxin, RelE toxin, and RelBE complex from *E. coli* in solution. We provide experimental evidence that the RelB protein lacks a well-ordered conformation in solution, whereas RelE is more rigid. This difference is also expressed in their differential thermal stabilities. We further demonstrated that a conformational fit is induced by the interaction of RelB and RelE, leading to significant thermodynamic and proteolytic stabilization of the system components. We verified that the bacterial RelB and RelE components share a similar secondary structure content with their orthologue archeal proteins. Nevertheless, we suggest that RelB is more similar to the CcdA family of antitoxins.

EXPERIMENTAL PROCEDURES

Expression and Purification of the RelB:His−*RelE Protein Complex*. RelB and His_6−RelE proteins were purified in complex from strain TOP10 harboring pSC2524HE (pA1/O4/O3::SDopt::*relB*;SDopt::*his*$_6$::*relE*) (to be published elsewhere). A 5 mL overnight culture was diluted in 2 L of 2× YT medium containing 100 mg/mL ampicillin (Amp) and was cultured at 37 °C. At $OD_{450} \approx 0.5$, the expression was induced by addition of 1 mM IPTG. After 4 h, the culture was harvested by centrifugation and resuspended in ice-cold buffer A (50 mM NaH_2PO_4, 0.3 M NaCl, 10 mM imidazole, 5 mM *β*-mercaptoethanol, pH 8; supplemented with two tablets of Complete EDTA-free protease inhibitor cocktail (Roche Molecular Biochemicals)). The cells were disrupted by passing them three times through a French press cell, and the soluble fraction was isolated by centrifugation for 30 min at 48400*g*. The cleared lysate was incubated with Ni−NTA agarose resin (Qiagen) in batch according to the manufacturer's instructions and subsequently loaded onto a gravity flow column at 4 °C. The Ni agarose resin was washed extensively in buffer B (50 mM NaH_2PO_4, 0.3 M NaCl, 35 mM imidazole, 1 mM *β*-mercaptoethanol, pH 8). Finally, the RelB:His−RelE complex was eluted in buffer B, 250 mM imidazole, and dialyzed against PBS (10 mM Na_2HPO_4, 2 mM KH_2PO_4, 137 mM NaCl, 27 mM KCl, pH 7.4), 10% glycerol, 5 mM DTT.

Purification of RelB. RelB was purified essentially as described for the RelB:His−RelE complex but with the following modifications: After the resin was washed in buffer B, RelB was eluted in two column volumes of buffer C (100 mM NaH_2PO_4, 10 mM Tris−HCl, 9.8 M urea, 1 mM *β*-mercaptoethanol, pH 8). The protein was concentrated, dialyzed against buffer Q (20 mM Tris−HCl, pH 8, 20 mM NaCl), and applied to a 1 mL HiTrap Q HP anion exchange column (Amersham Pharmacia). RelB was eluted using stepwise elution in buffer Q + NaCl and dialyzed against RelB storage buffer (25 mM Tris, pH 8, 100 mM KCl, 1 mM EDTA, 1 mM DTT, 10% glycerol).

Purification of His_6−RelE. The remaining His_6−RelE bound to the column from the above protocol was eluted in buffer D (100 mM NaH_2PO_4, 10 mM Tris−HCl, 9.8 M urea, 250 mM imidazole, 1 mM *β*-mercaptoethanol, pH 8). The protein was diluted and dialyzed against buffer SP (50 mM Hepes, pH 6, 50 mM NaCl), applied to a 1 mL HiTrap SP HP cation exchange column, and eluted using stepwise elution in buffer SP + NaCl. His_6−RelE was dialyzed into RelE storage buffer (3× PBS, pH 7.4, 10% glycerol, 5 mM DTT). Each purified protein was at least 95% pure as estimated by silver staining of SDS−PAGE gels. The molecular masses of the proteins were verified by matrix-assisted laser desorption ionization time-of-flight MS (MALDI-TOF MS). Prior to further analysis, all protein samples were dialyzed against PBS, pH 7.3, at 4 °C and centrifuged for 10 min at 12000*g* to remove insoluble protein aggregates.

Circular Dichroism (CD) Spectroscopy. CD spectra were obtained using an AVIV 202 spectropolarimeter equipped with a temperature-controlled sample holder and a 10 mm path length cuvette. The mean residual ellipticity, [*θ*], was calculated as $[\theta] = (100\theta m)/(cL)$, where *θ* is the observed ellipticity, *m* is the mean residual weight, *c* is the concentration (mg/mL), and *L* is the path length (cm). All experiments were performed in PBS, pH 7.3. For wavelength scan experiments, each spectrum represents the average of at least two scans. For thermal denaturation experiments, samples were equilibrated at each temperature step for at least 1 min, and the CD ellipticity was averaged for 1 min. Evaluation of the secondary structure composition obtained from far-UV CD spectra was facilitated by using the K2d, Selcon3, ContinLL, and CDsstr programs (*47*−*50*).

Fourier Transform Infrared (FTIR) Spectroscopy. Infrared spectra were recorded using a Nicolet Nexus 470 FTIR spectrometer with a DTGS detector. The protein sample, dissolved in PBS, pH 7.3, was suspended on a CaF_2 plate. The peptide deposit was resuspended in D_2O and then dried.

The resuspension procedure was repeated twice to ensure maximal hydrogen/deuterium exchange. The measurements of the 1600−1700 amide I region were taken using a 4 cm^{-1} resolution and 2000 scan average. The absorbance spectrum was deconvulated, and maximum values were determined by the PeakFit analysis software by autofitting the peaks using the first derivative (Seasolve). The secondary structure composition was estimated according to Byler and Susi (*51*) and Haris and Chapman (*52*).

Size Exclusion Chromatography (SEC) Analysis. Prior to each SEC analysis, protein samples were centrifuged (10 min, 15000*g*, 4 °C) to remove insoluble material. The SEC column used was a Superdex 75 10/300 (GE Healthcare Bio-Sciences). The samples were eluted at a flow rate of 1 mL/min at ambient temperature with PBS, pH 7.3. Protein elution was monitored at 280 nm.

Cloning, Expression, and Growth Rate Analysis of Truncated RelB and RelE Proteins. DNA fragments containing the coding sequence of the *relB*−*relE* gene pair, truncated *relB*−*relE* gene pair, and *relE* gene were produced by PCR using the chromosomal DNA of *E. coli* K-12 MG1655 as a template and the primers RelB1(*Nco*I)for (5′-TACCATGGGTAGCATTAACCTGC-3′), RelB36(*Nco*I)for (5′-TCCCATGGTCGAGTATATCGCTGAC-3′), RelB52(*Bsr*GI)for (5′-CATGTACAAGTGATGAAGATGCTGAAC-3′),RelE(*Nco*I)for (5′-TCCCATGGCGTATTTTCTGG-3′), and RelE(*Hin*dIII)-rev (5′-CTTAAGCTTTCAGAGAATGCGTTTGACCG-3′). The PCR fragments were cloned into the pBAD vector (Invitrogen) using suitable restriction enzymes to generate pBAD−RelBE, pBAD−$RelB_{36}$E, pBAD−$RelB_{52}$E, and pBAD−RelE. The plasmids were transformed into an *E. coli* TOP10 strain (Invitrogen). For the growth rate analysis experiment, the bacteria were cultured overnight in LB broth supplemented with 100 μg/mL ampicillin at 37 °C added with 0.4% D-glucose. The next day, the cultures were diluted and adjusted to an absorbance of ∼0.01 (A_{600}) in LB−ampicillin. Next, each culture was divided into two equal volumes; at time zero, the first half was added with 0.2% L-arabinose to induce expression of the target gene and the second half with 0.2% D-glucose to suppress low transcription from the pBAD promoter. All cultures were grown at 37 °C/200 rpm, and samples were taken sequentially approximately every 30 min. The cell density was measured by its absorbance at 600 nm.

Enzymatic Footprinting. Trypsin proteolysis of RelB, His−RelE, and the RelB:His−RelE complex was carried out by incubating 60 μg of purified protein with 0.6 μg of porcine trypsin (Promega) in trypsin resuspension buffer (50 mM acetic acid) in a total volume of 180 μL in 1× reaction buffer (50 mM Tris−HCl, pH 7.6, 1 mM $CaCl_2$) at 37 °C. Aliquots of 30 μL were withdrawn from each reaction mixture, and the reaction was terminated by addition of 10% TCA. The samples were stored on ice and subsequently centrifuged at 14000 rpm for 20 min at 4 °C. The protein pellet was resuspended in 1× SDS loading buffer, 50 mM DTT, loaded onto a NuPAGE (Invitrogen) 10% Bis-Tris gel, and subjected to electrophoresis in MES running buffer. The gels were finally stained with Coomassie Brilliant Blue R250. For the mass spectrometric peptide mass mapping of limited digestion, 4 μL of RelB or RelBE complex (both at 0.25 mg/mL in 150 mM KCl, 50 mM Tris, pH 8.0) was loaded onto a 5 mm column of immobilized trypsin (Poroszyme, Applied Biosystems) packed in the capillary end of a restricted Eppendorf GELoader pipet tip (*53*) at 25 °C and a flow of 25 μL/min, controlled by a peristaltic pump (P-1 from

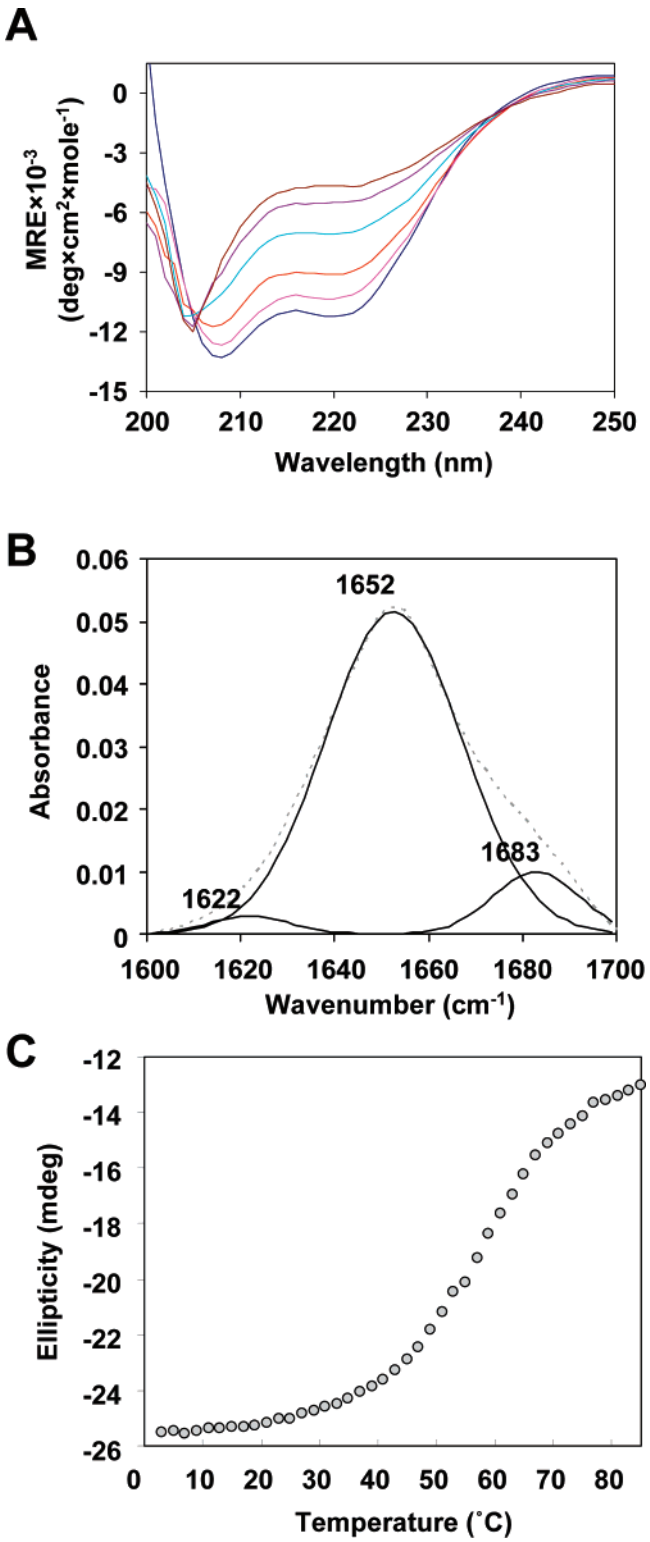

FIGURE 1: Structural analysis of RelB. (A) Far-UV CD analysis at 4 °C (blue), 37 °C (pink), 50 °C (red), 60 °C (turquoise), 70 °C (violet), and 80 °C (brown). The protein concentration was 4.8 μM. (B) FT-IR characterization at room temperature. The obtained spectrum of RelB (dashed line) was deconvoluted into three Gaussian-shaped spectra (solid lines), displaying maximum points at wavenumbers as indicated. (C) Thermal melt analysis (3−85 °C) of RelB monitored by CD ellipticity at 220 nm. The temperature step was 2 °C.

Table 1: Secondary Structure Contents (%) Determined from CD Spectra[a]

	RelB				RelE				RelBE			
method[b]	α	*β*	*t*	*c*	α	*β*	*t*	*c*	α	*β*	*t*	*c*
K2d	34	16	50[c]		13	33	54[c]		44	17	39[c]	
Selcon3	29	8	26	37	21	41	18	20	43	12	19	26
ContinLL	26	9	27	38	13	29	24	34	43	14	17	26
CDsstr	40	18	24	18	9	35	25	31	44	14	18	24
av	32.25	12.75	55		14	34.5	51.5		43.5	14.25	42.25	

[a] Key: α, α-helix; *β*, *β*-strand; t, *β*-turn or bend; c, random coil. [b] K2d, program developed by Andrade et al. (*47*); Selcon3, method developed by Sreerama et al. (*48*); ContinLL, method developed by Provencher and Glockner (*49*); CDsstr, method developed by Johnson (*50*). [c] Value includes random conformations and turns.

Pharmacia). A 0.5 μL portion of the digest was deposited onto a polished stainless steel MALDI target using the sandwich method with sinapinic acid (Fluka) as the matrix (*53*). The spectra were recorded on a Bruker Ultraflex MALDI-TOF instrument (Bruker) in the positive linear ion mode with delayed extraction.

Sequence Alignments and Structure Prediction. Sequence alignments were performed and similarity fractions were calculated using the T-COFFEE method (*54*) on the EBI server (http://www.ebi.ac.uk/t-coffee/). Secondary structure prediction was performed using the PSIPRED secondary structure prediction program (*55*) on the PSIPRED server (*56*).

RESULTS

RelB Antitoxin Characterization. To estimate the structure and thermodynamic stability of RelB antitoxin in solution, purified RelB was analyzed by FT-IR and far-UV CD spectroscopy at different temperatures. At low temperatures (4 °C) the far-UV spectral signatures of RelB antitoxin correspond to a typical α-helical pattern, indicated by minimum points at 208 and 222 nm (Figure 1A). Calculation of the secondary structure content was estimated to be approximately 32% α-helix, 13% *β*-sheet, and 55% turn and coil conformations (Table 1). The FT-IR spectrum of RelB at ambient temperature correlated with this finding, with a major amide I peak at 1652 cm^{-1} corresponding to predominantly α-helix content. The minor bands at 1683 and 1622 cm^{-1} correspond to *β*-strands as well as *β*-turns and bends (Figure 1B). The major band at 1652 cm^{-1} is rather broad and overlaps other bands. Indeed, second-derivative spectra of RelB revealed more minor bands at 1639, 1643, and 1666 cm^{-1} of unordered and turn portions (data not shown). Upon a temperature increase, a gradual structural unfolding was observed in CD with a T_M point of 58.5 °C, whereas at 80 °C the RelB spectrum predominantly correlated with a random coil conformation (Figure 1A). In the concentrations examined (4.8 μM), the RelB protein exhibited complete structural refolding, displaying an identical far-UV spectrum before and after exposure to 85 °C (data not shown). In addition, RelB CD samples stayed clear after being heated to 85 °C, suggesting that the RelB protein is thermostable. However, at higher concentrations (>20 μM), heating the RelB sample did result in some turbidity, indicating that its stability is concentration dependent.

His−RelE Toxin Characterization. The secondary structure content of the His−RelE protein, estimated by CD spectroscopy, featured the occurrence of both the α- and *β*-structures (Figure 2A), since minimum values were mainly located at 208 and 217 nm. Deconvolution of the CD spectra at 4 °C yielded an estimate of roughly 35% *β* and 14% α content (Table 1), suggesting that *β*-structures are more predominant. A high occurrence of turn and coil conformations (51%) was also reflected from the deconvolution analysis. FTIR analysis of purified His−RelE supported these findings, since the majority of wavenumber amide I bands were located between 1660 and 1700 cm^{-1}, with a major maximum at 1679 cm^{-1} and a minor band at 1636 cm^{-1} (Figure 2B), indicating a high amount of *β*-conformations (especially antiparallel *β*-sheets), *β*-turns, and bends, with a notably low number of α-structures and random coils (reflected by their low intensity from 1640 to 1660 cm^{-1}). CD thermal melt analysis revealed that the secondary structure content of RelE is rather stable and fully reversible between low and physiological temperatures (Figure 2C). At this temperature range, the observed structural changes may be ascribed to a modest decrease in α-helix content. At approximately 40 °C and above, an aggregation of RelE into insoluble sediments is observed, manifested by a sharp increase in CD ellipticity at 220 nm, with a thermal melting point of 52.5 °C. The RelE protein did not display structural refolding above 40 °C. Analyzing the soluble fraction of RelE at 4 °C after exposure to 50 °C revealed that the remaining soluble proteins (48% of the total proteins) could correctly refold (Figure 2A). However, such a partial refolding could not be observed after melting to 80 °C (data not shown).

His−RelE:RelB (RelBE) Toxin−Antitoxin Characterization. The far-UV CD and FTIR spectral patterns (Figure 3A,B and Table 1) show that the RelBE complex largely contains α-helices, coils, and a smaller amount of *β*-structures. Minimum bands at 208 nm and in the vicinity of 220 nm correlate with the presence of both α- and *β*-structures, whereas the significant negative CD band at 208 nm may suggest the contribution of coiled structures. The FTIR spectrum at the amide I region at ambient temperature is in line with this finding, exhibiting a major broad band at 1653 cm^{-1}, corresponding to the predominantly α-helical content, and minor bands at 1629 and 1682 cm^{-1}, corresponding to *β*-strands, antiparallel *β*-sheets, and turns. According to the CD thermal melt analysis (Figure 3C), the RelBE complex is quite thermostable, displaying a T_M point at 64.3 °C. Upon elevation of temperature, the *β*-sheet and coil structure part was increased on account of the α-helical content. Interestingly, following exposure to 90 °C, about 80% of the RelBE protein complex remained soluble and displayed refolding (data not shown), suggesting that the RelB antitoxin thermodynamically stabilized the RelE toxin. To assess whether the complex underwent a tertiary structural

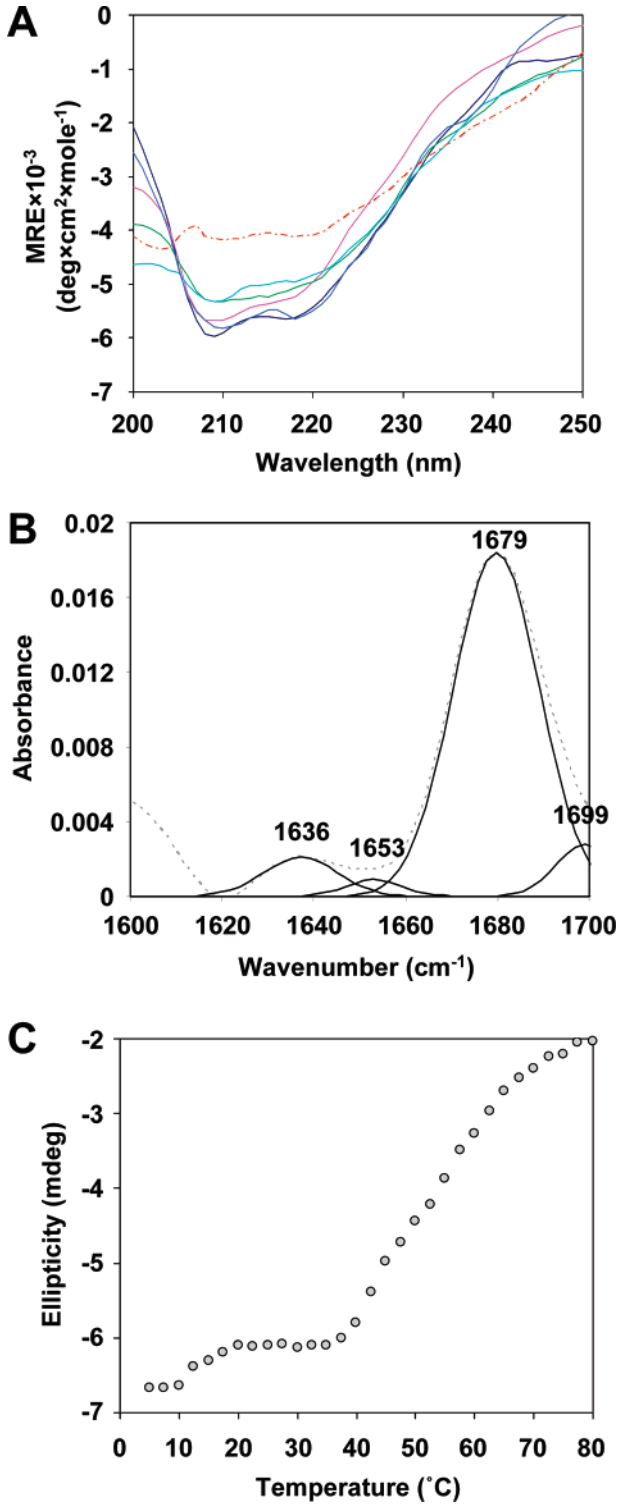

FIGURE 2: Structural analysis of His−RelE. (A) Far-UV CD analysis at 4 °C (blue), 15 °C (pink), 26 °C (green), 37 °C (turquoise), 50 °C (dashed red), and 4 °C after 50 °C (dark blue). The dashed line represents a turbid sample. The protein concentration was 2.6 μM. (B) FT-IR analysis at room temperature. The obtained spectrum of His−RelE (dashed line) was deconvoluted into several Gaussian-shaped spectra (solid lines), displaying maximum points at wavenumbers as indicated. (C) Thermal melt analysis (5−80 °C) of RelE monitored by CD ellipticity at 220 nm. The temperature step was 2.5 °C.

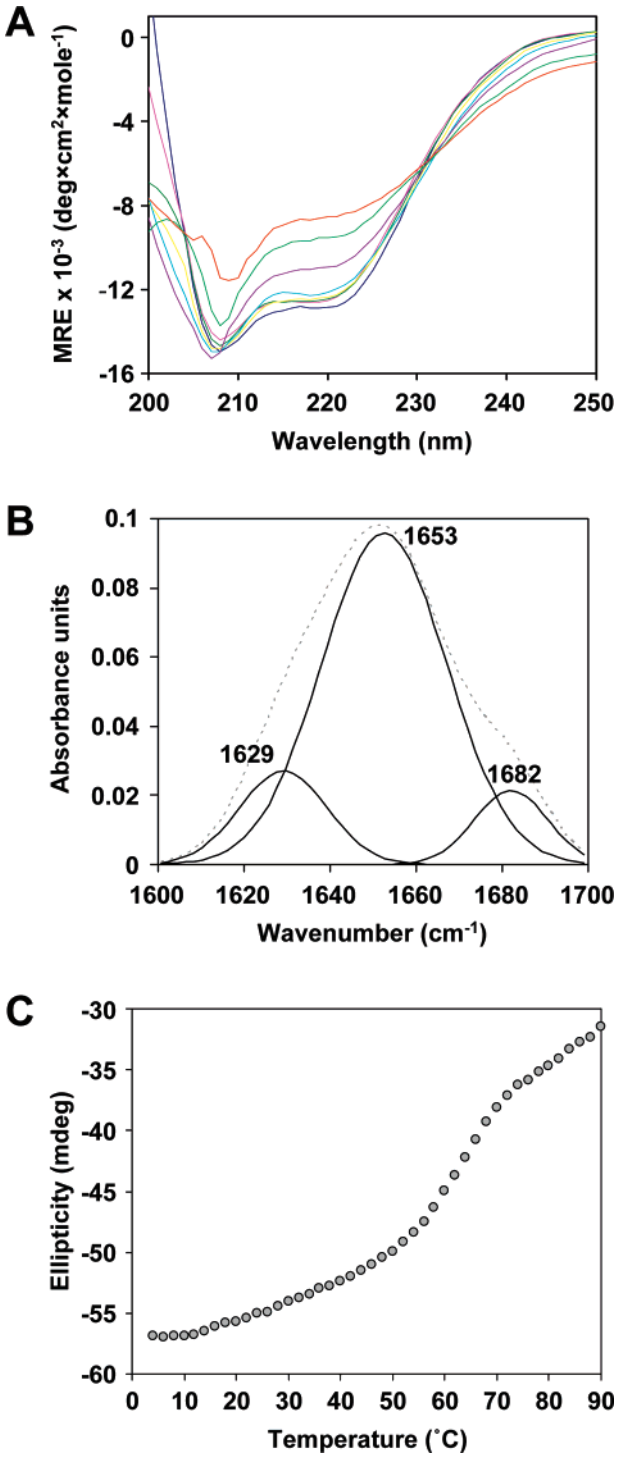

FIGURE 3: Structural analysis of the RelB:His−RelE complex. (A) Far-UV CD analysis at 4 °C (dark blue), 15 °C (pink), 26 °C (green), 37 °C (yellow), 48 °C (turquoise), 60 °C (violet), 80 °C (sea green), and 90 °C (red). The complex concentration was 0.6 μM. (B) FT-IR analysis at room temperature. The obtained spectrum of His−RelE (dashed line) was deconvoluted into three Gaussian-shaped spectra (solid lines), displaying maximum points at wavenumbers as indicated. (C) Thermal melt analysis (4−90 °C) of RelBE monitored by CD ellipticity at 220 nm. The temperature step was 2 °C.

change, the RelBE complex was analyzed in near-UV CD at 4, 37, 60, and 90 °C (Figure 4A) and the course of the total unfolding between 4 and 90 °C was monitored at 292 nm (Figure 4B). Up to a temperature of ~30 °C, the RelBE complex displayed a rather stable fold, with definite positive bands in the vicinity of 260 and 290 nm. However, between 30 and 53 °C a steady increase in ellipticity was observed, yet the spectral pattern featuring definite peaks at

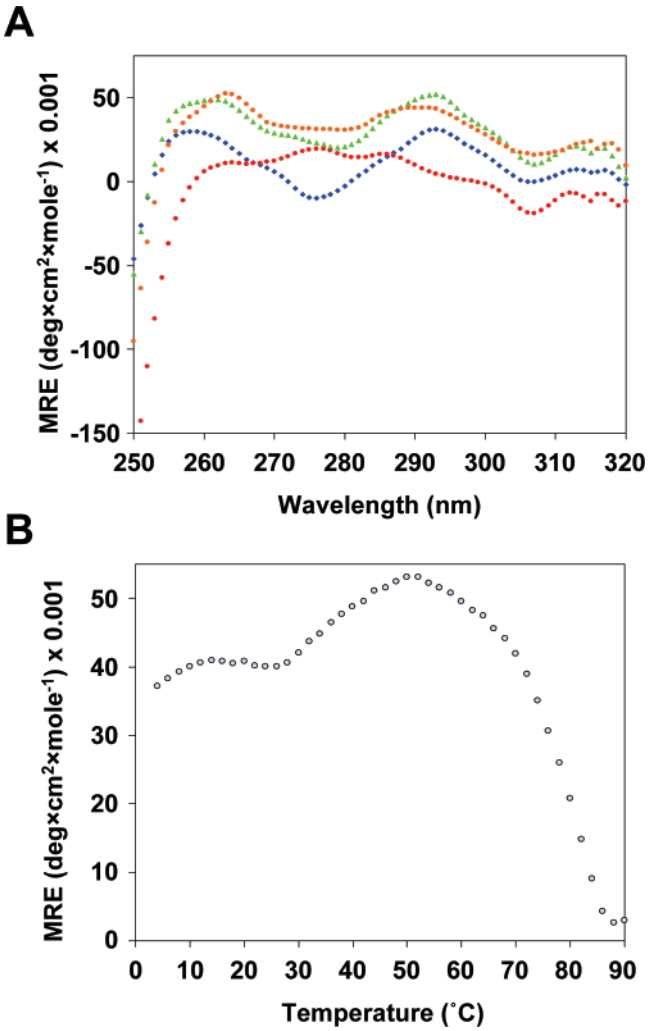

FIGURE 4: Near-UV CD analysis of the RelB:His−RelE complex. (A) The RelBE complex (8 μM) was analyzed at 4 °C (blue), 37 °C (green), 60 °C (orange), and 90 °C (red). The sample was equilibrated for 5 min at each temperature prior to measurement. (B) Thermal melt analysis (4−90 °C) of RelBE monitored by CD ellipticity at 292 nm. The temperature step was 2 °C.

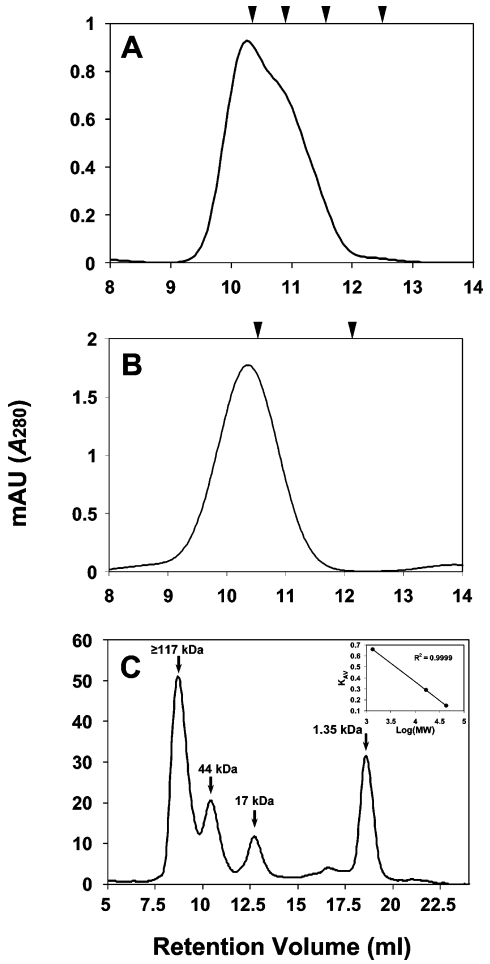

FIGURE 5: Size exclusion chromatography. (A) RelB antitoxin. Black arrowheads indicate the theoretical elution volumes for $(RelB)_2$, $(RelB)_3$, $(RelB)_4$, and $(RelB)_5$ stoichiometries. (B) RelBE complex. Black arrowheads indicate the theoretical elution volumes for His−RelE:RelB and $(His-RelE)_2$:$(RelB)_2$ stoichiometries. (C) Elution pattern of the protein standard (Bio-Rad). Protein molecular weights are indicated. The void volume retention time was further validated using blue dextran (MW ≈ 2 000 000). Inset: K_{av} vs log MW plot.

260 and 290 nm remained similar, suggesting that the tertiary structure of the protein underwent a certain change without exposure of their hydrophobic cores; otherwise the protein would have had a diminished absorbance of the aromatic residues. From 60 °C and above, a gradual loss in near-UV ellipticity suggested a formation of a molten globule state, until the near-UV spectral pattern was fully lost at 90 °C.

Oligomerization States of RelB and His−RelE:RelB (RelBE). To learn about the oligomerization state and three-dimensional compactness of the RelB and RelE proteins in solution, the proteins were loaded onto an analytical size exclusion column, using a Superdex 75 10/300 column. A protein concentration of approximately 10 μM (0.1 and 0.2 mg/mL RelB and RelBE, respectively) was selected for the analyses, because such a concentration is sufficiently low to avoid nonspecific aggregation, on one hand, yet is suitable for providing low but plausible detector readings at 280 nm, on the other hand. Size exclusion analysis of RelB antitoxin (60 μg, MW = 9071) yielded an asymmetric single broad peak with a maximum at a volume which is in line with an apparent weight of 49 550 (Figure 5A). Interestingly, the elution profile of RelB corresponds for apparent molecular weights that are significantly larger than the expected weight of a dimer (as many other antitoxins display) and even a trimer, and more close to that of a tetramer and a pentamer. The SEC technique is less informative for the determination of exact stoichiometries when dealing with nonglobular proteins. The RelBE complex (100 μg, MW = 21 119) eluted in a single peak with an apparent molecular weight of 46 651 (Figure 5B), which fit well with the $(RelB/His-RelE)_2$ stoichiometry in case the complex is indeed globular. Owing to the aggregative nature of the RelE protein, we were not able to analyze RelE using size exclusion chromatography. An attempt to resolve the His−RelE protein (70 μg, 12 048 Da) resulted in noisy detection of multiple high molecular weight aggregates (data not shown).

The Antitoxic Activity Resides in the RelB C-Terminal Region. To determine the region within RelB that is responsible for RelB−RelE interaction and antitoxic activity, full-length RelB ($RelB_{1-79}$) and two N-terminus-truncated antitoxin sequences ($RelB_{36-79}$ and $RelB_{52-79}$) were coexpressed with RelE toxin in a single operon using the pBAD promoter control. *E. coli* strain TOP10 cells, carrying the plasmids, were grown in LB medium, and 0.2% arabinose

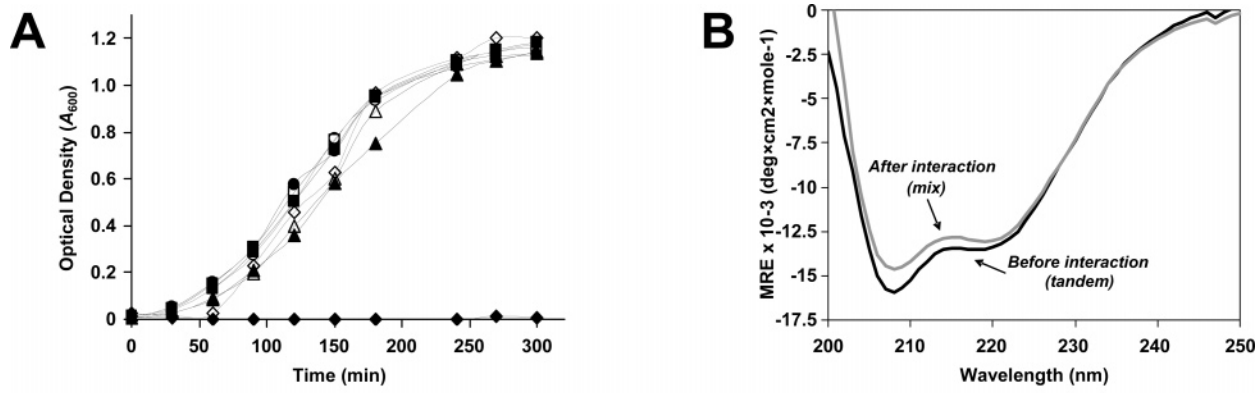

RelB 1-79: MGSINLRIDDELKARSYAALEKMGVTPSEALRLMLEYIADNERLPFKQTLLSDEDAELVEIVKERLRNPKPVRVTLDEL

RelB 36-79: MVEYIADNERLPFKQTLLSDEDAELVEIVKERLRNPKPVRVTLDEL

RelB 52-79: MGSGSGDDDDKLALMNCTSDEDAELVEIVKERLRNPKPVRVTLDEL

FIGURE 6: RelB−RelE interaction. (A) Identification of the RelB interaction region: *E. coli* strain TOP10 carrying one of the pBAD vectors expressing full-length RelB−RelE (■), $RelB_{36-79}$−RelE (▲), and $RelB_{52-79}$−RelE (●) together in a single operon were grown in LB−ampicillin medium at 37 °C, and growth curves were recorded. Transcription of the respective genes was induced by the addition of 0.2% arabinose at time zero (closed symbols). The amino acid sequences of the respective antitoxin components are shown in the lower panel (amino acids that are derived from the vector and do not belong to the RelB sequence itself are colored in gray). In parallel, equal culture volumes were added with 0.2% glucose as a negative control (open symbols). As a positive control, RelE (◆) expression was induced in the same system. (B) Conformational change following complex formation. Far-UV CD spectra of 2 μM RelB and 2 μM His−RelE before and after mixing in a tandem cell cuvette. The experiment was performed at 4 °C.

was added at time zero. The growth rate observed for $RelB_{36-79}$:RelE- or $RelB_{52-79}$:RelE-expressing bacteria was indifferent from that of the full-length-RelB:RelE-expressing bacteria (Figure 6A). As a positive control, expression of the RelE toxin using the same pBAD system led to significant growth arrest. The result suggests that RelB interacts and neutralizes RelE toxicity via its C-terminal region. The exact binding domain should be therefore located in the last 28 residues of RelB.

Conformational Changes during RelB−RelE Interactions. To determine whether the RelB and RelE proteins undergo a conformational change following their interaction, equimolar ratios of RelB and His−RelE proteins were examined by far-UV CD before and after interaction. The analysis was facilitated by the use of a tandem CD cuvette. As seen in Figure 6B, the two obtained CD spectra did not overlap, indicating that a structural change occurred following their interaction. Secondary structure content deconvolution of the spectra suggested a moderate transition of random coils (28.5% → 24%) to α-helices (38% → 41%) and β-turns (18% → 20.5%). The latter transition may explain the observed decrease in the absolute CD signal after interaction. It is likely that interactions induced structural changes that stabilized the flexible regions mainly within the antitoxin interaction domain.

RelB-Bound His−RelE Protects RelB from Proteolytic Cleavage. Further structural probing was carried out using trypsin-mediated proteolysis of free RelB, His−RelE, and the RelB:His−RelE complex. RelB degradation occurred through a metastable intermediate of a size corresponding to approximately 90% of full-length RelB (Figure 7A). Degradation of His−RelE went through a defined intermediate of approximately MW = 6000 which is visible after 30 min of digestion. In complex with His−RelE, full-length RelB is visible even at 60 min of incubation, indicating that His−RelE protects RelB against proteolytic cleavage. Additional bands appearing after 10 and 30 min of cleavage presumably correspond to intermediates of RelB (upper arrow) and His−RelE (lower arrow), respectively.

To further determine which part of RelB is sensitive to trypsin cleavage, we performed a MALDI-TOF MS analysis of a tryptic digest of free RelB (Figure 7B, upper panel) and RelB + His−RelE in equimolar quantities (Figure 7B, lower panel). Prior to MALDI ionization, samples were desalted and concentrated on a Poros R1 microcolumn (Experimental Procedures). The resulting spectrum contains a minor peak at *m*/*z* 8941 which corresponds to the average mass of a singly charged positive species of RelB lacking the N-terminal methionine residue. The base peak with an *m*/*z* value of 7309 corresponds to a tryptic fragment of RelB lacking the last 14 amino acid residues of the C-terminus (Figure 7C). This indicates that the C-terminus of RelB is more prone to proteolysis than the rest of the protein. In contrast, when the same amount of RelB was preincubated with His−RelE prior to trypsin digestion, a significant increase in the amount of uncleaved RelB appeared (Figure 7B, lower panel). This is consistent with the above results, showing His−RelE-mediated protection of RelB cleavage (Figure 7A). Thus, His−RelE protects the C-terminus of RelB against trypsin cleavage, suggesting that this part of RelB interacts and becomes structured upon binding to His−RelE.

DISCUSSION

Whereas the cellular activity of the RelBE TA system components and their physiologic importance were extensively studied, the structural and thermodynamic properties of the *E. coli* RelB and RelE proteins in solution remain to be determined. This characterization is highly important for a truly mechanistic understanding at the molecular and

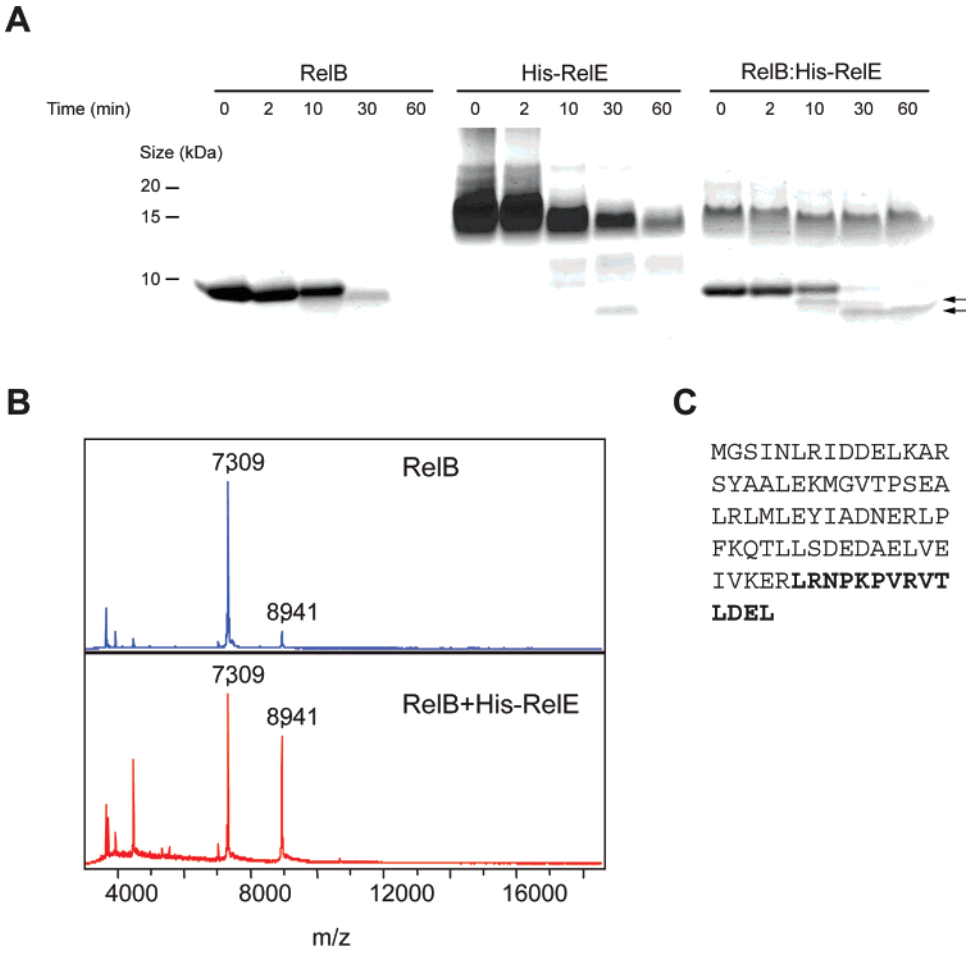

FIGURE 7: Structural probing: limited proteolysis with trypsin. (A) SDS−PAGE analysis of RelB, His−RelE, and the RelB:His−RelE complex digested with trypsin. The proteins were mixed at a 50× molar excess with trypsin and incubated at 37 °C. Samples were taken at the times indicated, and reactions were terminated by TCA precipitation and subsequently analyzed by SDS−PAGE. Arrows indicate the presence of degradation intermediates. (B) MALDI-TOF MS of a limited tryptic digest of RelB (upper panel) and RelB + His−RelE (lower panel). This digestion was performed at 25 °C by applying the proteins through a capillary containing porous beads with immobilized trypsin at a constant flow. (C) Amino acid sequence of RelB. The sequence corresponding to the truncated protein (M + 7309) in (B) is marked in bold.

biochemical levels of these systems. Here we characterized these features and tried to shed light on their structure−function relationship and gene divergence.

Our CD and FT-IR analyses of RelB antitoxin indicate that RelB in solution is rich in α-helices and fairly poor in β-structures and possesses significant amounts of turns and coils (Table 1). This secondary structure composition correlates somewhat with the structural composition of the crystallized aRelB protein, which shares 22% identity and 48% similarity with its bacterial homologue, RelB (Figure 8). However, it appears that RelB, at least in the non-toxin-binding state, is more populated with coils (55%) and contains less α-helix content (32% vs 60%). The high thermal stability of RelB supports the lack of an ordered fold and the presence of unordered region(s), since proteins including such regions are less susceptible to thermal aggregation due to the lack of hydrophobic patches being exposed to solvents during heating (*57*). Furthermore, the presence of disordered regions prevents the protein from folding into a globular conformation. According to our SEC analysis of RelB antitoxin, it displays exceptionally high molecular weights in solution. It is likely that these elevated molecular weights are due to the presence of disordered regions, occupying a high hydrodynamic radius. These findings correspond to the estimation of Takagi et al. that aRelB is less structured when it is not binding the toxin, owing to its apparent lack of a distinct hydrophobic core (*29*, *58*). It is expected that this feature, as in the case of other antitoxins, guarantees a high turnover rate of free RelB due to the action of the Lon protease (*12*). Indeed, recent half-life measurements of RelB expressed from the chromosome show half-lives in the range of 2−4 min (Overgaard and Gerdes, unpublished data).

Interestingly, the RelB, ParD, and CcdA antitoxins, despite their rather weak amino acid sequence similarity (8% identity and 26% similarity according to multiple sequence alignment), all demonstrate remarkable similarity in their far-UV CD signature, thermal melting pattern, and secondary structure prediction (*31*, *34*, *39*). ParD and CcdA proteins were structurally and thermodynamically characterized in detail and were suggested to belong to the same fold family (*31*, *33*, *34*, *36*, *39*, *59*). Therefore, it is possible that RelB antitoxin is structurally more similar to CcdA and ParD (as already had been suggested in the past (*31*)) than to aRelB. Similar to RelB, the ParD protein was estimated to be predominantly α-helical and include approximately 35% α- and 10% β-structures. These structures are located in the N-terminal region (*31*, *39*). The occurrence of a significant

FIGURE 8: Secondary structure content of RelB, RelE, and related proteins. Assignment of structures to amino acid sequences is based on secondary structure prediction by the PSIPRED method and according to the X-ray or NMR structure if available (PDB IDs are indicated: 1WMI (*29*); 2ADL (*33*); 2A6Q and 2A6S (*25*), 1MVF (*27*); 3VUB (*35*); 1UB4 (*24*)). The α-helices and extended strands are represented by rectangles and arrows, respectively. Sequences assigned with similar secondary structure alignment are shaded together in gray boxes. The asterisk signifies that the presented secondary structure is in a toxin−antitoxin complex.

disordered region in the C-terminus was also evident by NMR relaxation measurements of ^{15}N-labeled ParD (*31*). Likewise, the CcdA protein displayed a very similar CD signature (*34*). Moreover, the calculated secondary structure content of RelB is in good agreement with the 3D NMR secondary structure content of CcdA (*33*). The melting temperatures of RelB, ParD, and CcdA at physiological pH values are rather proximate (58.5, 60.7, and 54.2 °C, respectively), with very similar melting curve patterns (*34*, *39*). Furthermore, the secondary structure to sequence assignments (predicted and/or determined) of RelB, CcdA, and ParD are alike, whereas those of RelB and aRelB differ more (Figure 8). It is therefore possible that aRelB and RelB, despite their sequence homology, diverged to fit their "new" hosts. Indeed, examples of such an event were demonstrated in the case of the pTC-F14 and pTF-FC2 *pas* systems (*60*) and recently in the cases of the *E. coli* and *Streptococcus pneumoniae yefM*−*yoeB* systems (*61*) and the F plasmid and *E. coli* O157:H7 *ccd* systems (*62*), where, despite their high sequence homology, structural divergence prevented the recognition between antitoxins and toxins of the paralogue systems. According to both CcdA and ParD analyses, the unstructured region is included within their C-termini. We showed that the RelB interaction domain with RelE resides in the C-terminal third of the protein. Structural probing of RelB, RelE, and the RelBE complex using trypsin confirmed that the C-terminal part of RelB is sensitive to protease cleavage in its free state, while when complexed to RelE it becomes protected from proteolysis. Taken together, our results question whether bacterial RelB−RelE and archeal aRelB−aRelE interact similarly. Accordingly, RelB should include an unfolded C-terminus part that binds to the RelE toxin rather than the entire molecule (as in the case of aRelB). On this basis, it would be interesting to examine whether RelB can complement the activity of aRelB.

Our spectroscopic analyses indicate that the RelE conformation is compatible with the crystal structure of aRelE that is enriched in β-structures, particularly antiparallel β-sheets, and a large number of turns and inter-β-sheet loops. Further supported by their sequence homology (19% identity and 63% similarity) and predicted secondary structures (Figure 8), it is likely that RelE and aRelE have similar 3D structures. However, a lower α content is found in RelE, suggesting that part of the helical regions favor a β-conformation or coiled conformation in solution or in the nonbound state. Intriguingly, aRelE and YoeB display comparable 3D crystal structures, but different thermodynamic properties. While RelE is marginally thermostable above physiological temperatures, YoeB exhibits full reversibility up to 56 °C (*22*). The fact that RelE is very sensitive to elevated temperatures suggests that it cannot endure exposure of its hydrophobic core. A heat-induced conformational change leads to aggregation rather than transition into a molten globule state. Taken together, it is likely that RelE contains a well-structured hydrophobic core in solution as shown in the crystallized state of aRelE. Such a conformation is important in bestowing RelE with sufficient resistance to degradation on the one hand and in allowing it to execute an elaborate function on the other hand.

The formation of the RelB−RelE complex stabilized the toxin, and RelB−RelE actually displayed a higher thermal melting than RelB. The structural analysis of the complex suggested a gain of ordered structures at the expense of random coils. It is plausible that, upon complex formation, random coil regions within the RelB protein undergo structural transition into α-helices that are stabilized by the RelE interaction. These are similar to the conformational changes reported with CcdA−CcdB interactions (*36*) and are suggested for ParD (*31*) and YefM (*29*). Moreover, this interaction stabilized RelE and prevented it from aggregation above physiological temperatures, leading to substantial interaction-dependent stabilization, where the complex is more thermally stable than each of the components are separately. The thermodynamic stabilities of the two proteins separately and in complex may be adjusted to allow them to carry out their functions under different conditions: whereas a stable complex is required for the regulatory function, sizable differential stabilities are crucial for their toxin/antitoxin activities.

From the determination and/or prediction of the structures of seven well-studied TA members (Figure 8), it appears that in many cases (i) related antitoxins of structurally homologous toxins are not structurally similar (e.g., CcdA and MazE) and vice versa (e.g., YoeB and Doc) (this phenomenon was comprehensively discussed in the past (*63*) and proposed to result from mixing and matching events of toxin and antitoxin genes) and (ii) structural homology may not always guarantee sequence homology (e.g., CcdB and MazF) and vice versa (e.g., RelB and YefM). Furthermore, high homology may also reside within only part of the antitoxin sequences (e.g., the N-terminal regions of YefM and Phd, and YefM from *E. coli* and *S. pneumoniae*), whereas the rest of the sequence differs to some extent, leading to a marked overall change of structure and dynamic characteristics (*30*, *38*, *61*). We hypothesize that this is the case in RelB and aRelB antitoxins. We postulate that the adjustment of the antitoxin sequence in every host is important to achieve DNA binding, thermodynamic and proteolytic stability properties suitable to each host on the one hand, and proper toxin−antitoxin recognition on the other hand.

CONCLUSIONS

Our study provides structural insights into the structure and thermodynamics of RelB and RelE in solution. We showed evidence that (i) RelB possesses a high content of α-helical and flexible regions and exhibits a conformationally induced fit upon toxin binding, as many proteins featuring disordered regions do, (ii) RelE is a well-folded protein, displaying a high content of antiparallel β-sheets and β-turns, (iii) RelB, RelE, and the RelBE complex display considerably different thermodynamic stabilities that most likely serve as an important functional basis that regulates the activity of the system under different conditions, (iv) the C-terminal part of RelB is responsible for RelB−RelE interaction, and (iv) the C-terminal part of RelB is likely to be unfolded due to high sensitivity to protease activity and this part interacts with RelE to become more resistant to degradation. On the basis of our analyses, we further suggest that RelB is structurally similar to the CcdA and ParD proteins; however, complementary experiments are required to verify the exact RelB structure.

ACKNOWLEDGMENT

We thank the laboratory members for helpful discussions.

REFERENCES

1. Engelberg-Kulka, H., and Glaser, G. (1999) Addiction modules and programmed cell death and antideath in bacterial cultures, *Annu. Rev. Microbiol. 53*, 43−70.
2. Gerdes, K., Christensen, S. K., and Lobner-Olesen, A. (2005) Prokaryotic toxin-antitoxin stress response loci, *Nat. Rev. Microbiol. 3*, 371−382.
3. Hayes, F. (2003) Toxins-antitoxins: plasmid maintenance, programmed cell death, and cell cycle arrest, *Science 301*, 1496−1499.
4. Pedersen, K., Christensen, S. K., and Gerdes, K. (2002) Rapid induction and reversal of a bacteriostatic condition by controlled expression of toxins and antitoxins, *Mol. Microbiol. 45*, 501−510.
5. Amitai, S., Yassin, Y., and Engelberg-Kulka, H. (2004) MazF-mediated cell death in Escherichia coli: a point of no return, *J. Bacteriol. 186*, 8295−8300.
6. Buts, L., Lah, J., Dao-Thi, M. H., Wyns, L., and Loris, R. (2005) Toxin-antitoxin modules as bacterial metabolic stress managers, *Trends Biochem. Sci. 30*, 672−679.
7. Engelberg-Kulka, H., Amitai, S., Kolodkin-Gal, I., and Hazan, R. (2006) Bacterial programmed cell death and multicellular behavior in bacteria, *PLoS Genet. 2*, e135.
8. Condon, C. (2006) Shutdown decay of mRNA, *Mol. Microbiol. 61*, 573−583.
9. Pandey, D. P., and Gerdes, K. (2005) Toxin-antitoxin loci are highly abundant in free-living but lost from host-associated prokaryotes, *Nucleic Acids Res. 33*, 966−976.
10. Christensen, S. K., and Gerdes, K. (2003) RelE toxins from bacteria and Archaea cleave mRNAs on translating ribosomes, which are rescued by tmRNA, *Mol. Microbiol. 48*, 1389−1400.
11. Christensen, S. K., Pedersen, K., Hansen, F. G., and Gerdes, K, (2003) Toxin-antitoxin loci as stress-response-elements: ChpAK/MazF and ChpBK cleave translated RNAs and are counteracted by tmRNA, *J. Mol. Biol. 332*, 809−819.
12. Christensen, S. K., Mikkelsen, M., Pedersen, K., and Gerdes, K. (2001) RelE, a global inhibitor of translation, is activated during nutritional stress, *Proc. Natl. Acad. Sci. U.S.A. 98*, 14328−14333.
13. Tsilibaris, V., Maenhaut-Michel, G., Mine, N., and Van Melderen, L. (2007) What is the benefit for E. coli to have multiple toxin-antitoxin systems in their genomes? *J. Bacteriol.* (in press).
14. Lewis, K. (2005) Persister cells and the riddle of biofilm survival, *Biochemistry (Moscow) 70*, 267−274.
15. Keren, I., Shah, D., Spoering, A., Kaldalu, N., and Lewis, K. (2004) Specialized persister cells and the mechanism of multidrug tolerance in Escherichia coli, *J. Bacteriol. 186*, 8172−8180.
16. Moritz, E. M., and Hergenrother, P. J. (2007) Toxin-antitoxin systems are ubiquitous and plasmid-encoded in vancomycin-resistant enterococci, *Proc. Natl. Acad. Sci. U.S.A. 104*, 311−316.
17. Gronlund, H., and Gerdes, K. (1999) Toxin-antitoxin systems homologous with relBE of Escherichia coli plasmid P307 are ubiquitous in prokaryotes, *J. Mol. Biol. 285*, 1401−1415.
18. Van Melderen, L., Bernard, P., and Couturier, M. (1994) Lon-dependent proteolysis of CcdA is the key control for activation of CcdB in plasmid-free segregant bacteria, *Mol. Microbiol. 11*, 1151−1157.
19. Lehnherr, H., and Yarmolinsky, M. B. (1995) Addiction protein Phd of plasmid prophage P1 is a substrate of the ClpXP serine protease of Escherichia coli, *Proc. Natl. Acad. Sci. U.S.A. 92*, 3274−3277.
20. Smith, A. S., and Rawlings, D. E. (1998) Efficiency of the pTF-FC2 pas poison-antidote stability system in Escherichia coli is affected by the host strain, and antidote degradation requires the lon protease, *J. Bacteriol. 180*, 5458−5462.
21. Christensen, S. K., Maenhaut-Michel, G., Mine, N., Gottesman, S., Gerdes, K., and Van Melderen, L. (2004) Overproduction of the Lon protease triggers inhibition of translation in Escherichia coli: involvement of the yefM-yoeB toxin-antitoxin system, *Mol. Microbiol. 51*, 1705−1717.
22. Cherny, I., Rockah, L., and Gazit, E. (2005) The YoeB toxin is a folded protein that forms a physical complex with the unfolded YefM antitoxin. Implications for a structural-based differential stability of toxin-antitoxin systems, *J. Biol. Chem. 280*, 30063−30072.
23. Aizenman, E., Engelberg-Kulka, H., and Glaser, G. (1996) An Escherichia coli chromosomal "addiction module" regulated by guanosine 3′,5′-bispyrophosphate: a model for programmed bacterial cell death, *Proc. Natl. Acad. Sci. U.S.A. 93*, 6059−6063.
24. Kamada, K., Hanaoka, F., and Burley, S. K. (2003) Crystal structure of the MazE/MazF complex: molecular bases of antidote-toxin recognition, *Mol. Cell 11*, 875−884.
25. Kamada, K., and Hanaoka, F. (2005) Conformational change in the catalytic site of the ribonuclease YoeB toxin by YefM antitoxin, *Mol. Cell 19*, 497−509.
26. Lah, J., Marianovsky, I., Glaser, G., Engelberg-Kulka, H., Kinne, J., Wyns, L., and Loris, R. (2003) Recognition of the intrinsically flexible addiction antidote MazE by a dromedary single domain antibody fragment. Structure, thermodynamics of binding, stability, and influence on interactions with DNA, *J. Biol. Chem. 278*, 14101−14111.
27. Loris, R., Marianovsky, I., Lah, J., Laeremans, T., Engelberg-Kulka, H., Glaser, G., Muyldermans, S., and Wyns, L. (2003) Crystal structure of the intrinsically flexible addiction antidote MazE, *J. Biol. Chem. 278*, 28252−28257.
28. Lah, J., Simic, M., Vesnaver, G., Marianovsky, I., Glaser, G., Engelberg-Kulka, H., and Loris, R. (2005) Energetics of structural transitions of the addiction antitoxin MazE: is a programmed bacterial cell death dependent on the intrinsically flexible nature of the antitoxins? *J. Biol. Chem. 280*, 17397−17407.
29. Takagi, H., Kakuta, Y., Okada, T., Yao, M., Tanaka, I., and Kimura, M. (2005) Crystal structure of archaeal toxin-antitoxin RelE-RelB complex with implications for toxin activity and antitoxin effects, *Nat. Struct. Mol. Biol. 12*, 327−331.
30. Cherny, I., and Gazit, E. (2004) The YefM antitoxin defines a family of natively unfolded proteins: implications as a novel antibacterial target, *J. Biol. Chem. 279*, 8252−8261.
31. Oberer, M., Zangger, K., Prytulla, S., and Keller, W. (2002) The anti-toxin ParD of plasmid RK2 consists of two structurally distinct moieties and belongs to the ribbon-helix-helix family of DNA-binding proteins, *Biochem. J. 361*, 41−47.
32. Hargreaves, D., Santos-Sierra, S., Giraldo, R., Sabariegos-Jareno, R., de la Cueva-Mendez, G., Boelens, R., Diaz-Orejas, R., and Rafferty, J. B. (2002) Structural and functional analysis of the kid toxin protein from E. coli plasmid R1, *Structure 10*, 1425−1433.
33. Madl, T., Van Melderen, L., Mine, N., Respondek, M., Oberer, M., Keller, W., Khatai, L., and Zangger, K. (2006) Structural basis for nucleic acid and toxin recognition of the bacterial antitoxin CcdA, *J. Mol. Biol. 364*, 170−185.
34. Dao-Thi, M. H., Messens, J., Wyns, L., and Backmann, J. (2000) The thermodynamic stability of the proteins of the ccd plasmid addiction system, *J. Mol. Biol. 299*, 1373−1386.
35. Loris, R., Dao-Thi, M. H., Bahassi, E. M., Van Melderen, L., Poortmans, F., Liddington, R., Couturier, M., and Wyns, L. (1999) Crystal structure of CcdB, a topoisomerase poison from E. coli, *J. Mol. Biol. 285*, 1667−1677.
36. Van Melderen, L., Thi, M. H., Lecchi, P., Gottesman, S., Couturier, M., and Maurizi, M. R. (1996) ATP-dependent degradation of CcdA by Lon protease. Effects of secondary structure and heterologous subunit interactions, *J. Biol. Chem. 271*, 27730−27738.
37. Gazit, E., and Sauer, R. T. (1999) The Doc toxin and Phd antidote proteins of the bacteriophage P1 plasmid addiction system form a heterotrimeric complex, *J. Biol. Chem. 274*, 16813−16818.
38. Gazit, E., and Sauer, R. T. (1999) Stability and DNA binding of the phd protein of the phage P1 plasmid addiction system, *J. Biol. Chem. 274*, 2652−2657.
39. Oberer, M., Lindner, H., Glatter, O., Kratky, C., and Keller, W. (1999) Thermodynamic properties and DNA binding of the ParD protein from the broad host-range plasmid RK2/RP4 killing system, *Biol. Chem. 380*, 1413−1420.
40. Parsell, D. A., and Sauer, R. T. (1989) The structural stability of a protein is an important determinant of its proteolytic susceptibility in Escherichia coli, *J. Biol. Chem. 264*, 7590−7595.
41. Gerdes, K. (2000) Toxin-antitoxin modules may regulate synthesis of macromolecules during nutritional stress, *J. Bacteriol. 182*, 561−572.
42. Motiejunaite, R., Armalyte, J., Markuckas, A., and Suziedeliene, E. (2007) Escherichia coli dinJ-yafQ genes act as a toxin-antitoxin module, *FEMS Microbiol. Lett. 268*, 112−119.

43. Pedersen, K., Zavialov, A. V., Pavlov, M. Y., Elf, J., Gerdes, K., and Ehrenberg, M. (2003) The bacterial toxin RelE displays codon-specific cleavage of mRNAs in the ribosomal A site, *Cell 112*, 131−140.
44. Dyson, H. J., and Wright, P. E. (2005) Intrinsically unstructured proteins and their functions, *Nat. Rev. Mol. Cell Biol. 6*, 197−208.
45. Tompa, P. (2005) The interplay between structure and function in intrinsically unstructured proteins, *FEBS Lett. 579*, 3346−3354.
46. Dyson, H. J., and Wright, P. E. (2002) Coupling of folding and binding for unstructured proteins, *Curr. Opin. Struct. Biol. 12*, 54−60.
47. Andrade, M. A., Chacon, P., Merelo, J. J., and Moran, F. (1993) Evaluation of secondary structure of proteins from UV circular dichroism spectra using an unsupervised learning neural network, *Protein Eng. 6*, 383−390.
48. Sreerama, N., Venyaminov, S. Y., and Woody, R. W. (1999) Estimation of the number of alpha-helical and beta-strand segments in proteins using circular dichroism spectroscopy, *Protein Sci. 8*, 370−380.
49. Provencher, S. W., and Glockner, J. (1981) Estimation of globular protein secondary structure from circular dichroism, *Biochemistry 20*, 33−37.
50. Johnson, W. C. (1999) Analyzing protein circular dichroism spectra for accurate secondary structures, *Proteins 35*, 307−312.
51. Byler, D. M., and Susi, H. (1986) Examination of the secondary structure of proteins by deconvolved FTIR spectra, *Biopolymers 25*, 469−487.
52. Haris, P. I., and Chapman, D. (1995) The conformational analysis of peptides using Fourier transform IR spectroscopy, *Biopolymers 37*, 251−263.
53. Kussmann, M., and Roepstorff, P. (2000) Sample preparation techniques for peptides and proteins analyzed by MALDI-MS, *Methods Mol. Biol. 146*, 405−424.
54. Notredame, C., Higgins, D. G., and Heringa, J. (2000) T-Coffee: A novel method for fast and accurate multiple sequence alignment, *J. Mol. Biol. 302*, 205−217.
55. Jones, D. T. (1999) Protein secondary structure prediction based on position-specific scoring matrices, *J. Mol. Biol. 292*, 195−202.
56. McGuffin, L. J., Bryson, K., and Jones, D. T. (2000) The PSIPRED protein structure prediction server, *Bioinformatics 16*, 404−405.
57. Receveur-Brechot, V., Bourhis, J. M., Uversky, V. N., Canard, B., and Longhi, S. (2006) Assessing protein disorder and induced folding, *Proteins 62*, 24−45.
58. Wilson, D. N., and Nierhaus, K. H. (2005) RelBE or not to be, *Nat. Struct. Mol. Biol. 12*, 282−284.
59. Magnuson, R., Lehnherr, H., Mukhopadhyay, G., and Yarmolinsky, M. B. (1996) Autoregulation of the plasmid addiction operon of bacteriophage P1, *J. Biol. Chem. 271*, 18705−18710.
60. Deane, S. M., and Rawlings, D. E. (2004) Plasmid evolution and interaction between the plasmid addiction stability systems of two related broad-host-range IncQ-like plasmids, *J. Bacteriol. 186*, 2123−2133.
61. Nieto, C., Cherny, I., Khoo, S. K., de Lacoba, M. G., Chan, W. T., Yeo, C. C., Gazit, E., and Espinosa, M. (2007) The yefM-yoeB toxin-antitoxin systems of Escherichia coli and Streptococcus pneumoniae: functional and structural correlation, *J. Bacteriol. 189*, 1266−1278.
62. Wilbaux, M., Mine, N., Guerout, A. M., Mazel, D., and Van Melderen, L. (2007) Functional interactions between coexisting toxin-antitoxin systems of the ccd family in Escherichia coli O157: H7, *J. Bacteriol. 189*, 2712−2719.
63. Anantharaman, V., and Aravind, L. (2003) New connections in the prokaryotic toxin-antitoxin network: relationship with the eukaryotic nonsense-mediated RNA decay system, *GenomeBiology 4*, R81.

BI701037E